Am J Transl Res 2023;15(7):4467-4486
www.ajtr.org /ISSN:1943-8141/AJTR0145296

Original Article

A composite hydrogel with antibacterial and promoted cell proliferation dual properties for healing of infected wounds

Shikun Wei[1,2*], Zhongshan Wang[2*], Xiaoyan Liang[3], Tingliang Xiong[1], Zhengyang Kang[1], Sheng Lei[1], Bin Wu[1], Biao Cheng[2]

[1]Department of Orthopedics, The Second People's Hospital of Panyu District, Guangzhou 511400, Guangdong, China; [2]Department of Burn and Plastic Surgery, General Hospital of Southern Theater Command, PLA, Guangzhou 510010, Guangdong, China; [3]The Affiliated Hexian Memorial Hospital of Southern Medical University, Guangzhou 511400, Guangdong, China. [*]Equal contributors.

Received July 12, 2022; Accepted June 8, 2023; Epub July 15, 2023; Published July 30, 2023

Abstract: Wound infection remains a major challenge for health professionals, because it delays wound healing and increases the overall cost and morbidity. Therefore, the development of new biomaterials with new antibacterial properties and healing effects remains a dire clinical need. To solve this problem, we developed silver nanoparticles embedded in γ-cyclodextrin metal-organic frameworks (Ag@MOF) and platelet-rich plasma (PRP)-loaded hydrogel systems based on methacrylated silk fibroin (SFMA) and methacrylate hyaluronic acid (HAMA) as Ag^+ ion and growth factor delivery vehicles for inhibiting the growth of drug-resistant bacteria and promoting wound healing. The prepared SFMA/HAMA hydrogel demonstrated good rheological properties, swelling capability, appropriate mechanical properties and controllable biodegradability. The SFMA/HAMA/Ag@MOF/PRP hydrogel showed sustained release profiles of Ag^+ ions and EGF. The SFMA/HAMA/Ag@MOF hydrogel have good inherent antibacterial properties against both gram-negative bacteria and gram-positive bacteria. The prepared hydrogel showed excellent cytocompatibility and could stimulate the growth and proliferation rate of NIH-3T3 cells. *In vivo* experiments showed that SFMA/HAMA/Ag@MOF/PRP hydrogel treatment enhanced the healing of full-thickness wounds, reduced inflammatory cell infiltration, and promoted re-epithelialization and collagen synthesis. All results indicated that the prepared hydrogel has tremendous potential to reduce wound infections and improve wound healing.

Keywords: Platelet-rich plasma (PRP), nanosilver, methacrylated silk fibroin (SFMA), methacrylate hyaluronic acid (HAMA), wound infection

Introduction

Chronic wound healing is one of the most common and difficult problems encountered by clinicians [1, 2]. Surgical debridement is the key to treating chronic wounds, but how to promote and accelerate wound healing after removal of infected and necrotic tissue is a challenge for every surgeon [3, 4]. The limited availability of autologous skin or flap grafts and the rejection of allogeneic skin grafts have promoted the search for novel bioalternative materials to treat wounds [5]. With the development of molecular biology techniques and materials science, a variety of natural biomaterials have been widely used in the treatment of chronic wounds and have achieved a certain effect [6, 7]. However, these common dressing materials without insufficient antimicrobial activity are not sufficient to eliminate bacterial infection. Bacterial infections at the wound tissue site usually delay the wound healing process or even lead to serious life-threatening complications [8, 9]. Therefore, it is now imperative to develop an efficient wound dressing to simultaneously enhance antimicrobial capacity and improve wound healing.

Silver nanoparticles with small particle sizes and large specific surface areas have been the research focus of antibiotics in recent years and have strong penetration, broad-spectrum

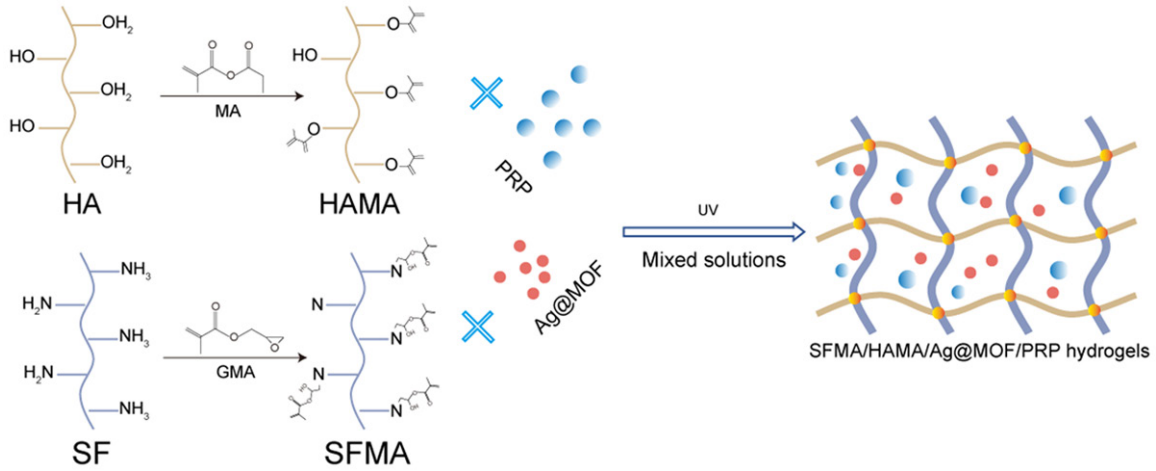

Scheme 1. Flow diagram of the preparation of the SFMA/HAMA/PRP/Ag@MOF hydrogel.

sterilization, unique antibacterial mechanisms and no drug resistance [10, 11]. Meanwhile, it can promote cell growth and wound healing and has no irritating reaction to the skin, which opens up prospects for the wide application of silver nanoparticles [12, 13]. However, dissolved silver ions have active chemical properties (easy to oxidize or agglomerate to form aggregates with large particle sizes), which limits their application [14, 15]. Metal-organic frameworks (MOFs), also known as porous coordination polymers, are crystalline porous materials composed of inorganic metal ions or clusters connected by multidentate organic ligands [16, 17]. MOFs may be of interest in biomedical applications, but they are often unstable in solutions containing physiological proteins [18]. Therefore, we can load MOFs into the hydrogel as a strategy to alleviate its degradation and prevent the premature release of silver ions so that silver-based MOFs (Ag@MOF) can be used to promote wound healing [19, 20].

Platelet-rich plasma (PRP) is a kind of concentrated plasma separated from blood that has large platelets, growth factors and a small amount of red blood cells [21, 22]. PRP has great potential in the field of regenerative medicine because of its low cost-effectiveness, wide source, low risk of infection and strong ability of therapeutic tissue regeneration. PRP contains a large amount of fibrinogen, which is activated by external stimulation to produce a large amount of fibrin and release a variety of growth factors (EGF, VEGF, IGF, TGF-β1, PDGF, etc.) [23-25]. These growth factors play a complementary role in a variety of regenerative medicine treatment programs for tissue repair, including the treatment of muscle and spinal diseases, osteoarthritis, chronic complex and intractable wounds [26]. Currently, there are some disadvantages in the clinical research of PRP. The main problem is the explosive release of PRP, which limits the long-term treatment of PRP [27]. In addition, due to the short bioactivity cycle of PRP *in vitro*, whether PRP can be loaded with hydrogels to prolong the bioactivity cycle to better promote wound healing is unknown [28, 29].

Silk fibroin (SF) and hyaluronic acid (HA) are natural hydrophilic colloids with good adhesion and biocompatibility. Natural polymers contain hydroxyl and amino groups, which can be chemically modified to improve mechanical properties and biological stability [30-32]. In this paper, HAMA was synthesized by modifying HA with methacrylic anhydride (MA), and SFMA was synthesized by modifying SF with glycidyl methacrylate (GMA) (**Scheme 1**). Then, in the presence of UV light and photoinitiator LAP, the SFMA/HAMA composite hydrogel was formed by mixing the SFMA solution and HAMA solution. Based on the biological functions and research background of Ag@MOF, PRP and modified hydrogels, this study proposed the hypothesis that SFMA/HAMA hydrogels could be used as silver ions and growth factor carriers. Material characterization, biocompatibility and a rat wound infection model were used to study and evaluate the mechanism and effect

of SFMA/HAMA/PRP/Ag@MOF in promoting wound healing.

Material and methods

Materials and reagents

Hyaluronic acid (HA) was purchased from Shanghai Yuanye Biotechnology Co., Ltd. (Shanghai, China). Sliced cocoons were purchased from Zhejiang Academy of Agricultural Sciences. γ-Cyclodextrin (γ-CD), KOH, methacrylic anhydride (MA), glycidyl methacrylate (GMA) and polyethylene glycol (PEG, Mw= 20,000) were purchased from Macklin Biochemical Technology Co., Ltd. (Shanghai, China). Silver nitrate ($AgNO_3$) was purchased from Sigma Aldrich Corporation (MO, USA). Platelet-rich plasma (PRP) was obtained from Army General Hospital of Guangzhou military region (Guangzhou, China). *Escherichia coli* (*E. coli*, ATCC8739) and *Staphylococcus aureus* (*S. aureus*, ATCC-14458) were obtained from Chuangsai Biomedical Material Co., Ltd. (Guangzhou, China).

Synthesis of methacrylated silk fibroin (SFMA)

The cocoons were cut into small pieces and added to 2 L Na_2CO_3 (0.02 M) solution and boiled for 45 min. The degummed SF was washed with deionized water three times and oven-dried at 60°C overnight. Then, 25 g of degummed SF was dissolved in 100 mL lithium bromide solution (9.3 M). When the filaments were completely dissolved, 15 mL GMA was added to the mixture and stirred at room temperature overnight. After the reaction, the solution was filtered through a miracloth (Miracloth) and dialyzed into a dialysis bag with a molecular weight of 3500 Da. After dialysis in distilled water for 3-5 days, the solution was lyophilized for 48 h to obtain SFMA.

Synthesis of methacrylate hyaluronic acids (HAMA)

HAMA was also synthesized following a previously published protocol [33]. 1 g of HA was dissolved in 100 mL of distilled water, followed by the addition of 3 mL of methacrylic anhydride into the HA solution. The pH of the reaction was adjusted to 8.5 by the addition of 5 mol/L NaOH and kept at room temperature under continuous stirring for 8 h. After dialysis in distilled water for 3-5 days, the solution was lyophilized for 48 h to obtain HAMA.

Synthesis of Ag@MOF

Nanosized CD-MOF crystals were generated following previously published protocols [34]. The Ag@MOF was prepared by impregnation reduction following a previously published protocol with slight modifications [35]. Briefly, 500 mg of CD MOF crystals was dispersed in 1 mL of acetonitrile, and then 4 mL of $AgNO_3$ (10 mM) was added and vigorously stirred. After stirring for 48 h, the reaction mixture was centrifuged and washed three times with acetonitrile and deionized water and then lyophilized to obtain Ag@MOF.

Preparation of SFMA/HAMA hydrogel

For the preparation of composite hydrogels, the concentration of SFMA in the PBS solution was fixed at 10 wt%, and varying concentrations of HAMA (0.5 wt%, 1.0 wt% and 1.5 wt%) in PBS solution were mixed in SFMA solution at a 1:1 volume ratio. LAP (0.1 wt%) was subsequently added as a photoinitiator. The mixture was then injected directly into 48-well culture plates and irradiated with 405 nm light for 30 s.

Characterization of the synthesized materials

SF, SFMA, HA and HAMA were characterized by ^1H NMR (AV-500, Bruker, Germany) in D2O. The morphological characteristics of Ag@MOF nanoparticles were analyzed using TEM (Libra 200, Carl Zeiss, Germany). After freeze-drying, the surface morphologies were characterized by scanning electron microscopy (SEM, S-3400, Hitachi, Japan).

Physical evaluation of the composite hydrogels

Swelling ratio of the hydrogels: SFMA/HAMA hydrogel samples with different HAMA concentrations were placed in PBS solution (pH=7.4). At defined intervals, the swollen hydrogels were removed and weighed. The calculation formula of the swelling ratio was as follows:

$$\text{Swelling ratio } (\%)=(W_t-W_0)/W_0\times 100\%$$

Where W_t is the weight of the sample at time t and W_0 is the weight of the hydrogel at time 0.

Rheological assessment: Rheological characterization was performed on a TA rheometer instrument (Malvern Instruments Ltd., Malvern, UK). Before the test, the hydrogel samples remained overnight at 4°C, and the storage modulus (G') and loss modulus (G") were measured at 25°C. In amplitude scanning, the test temperature was 25°C, and the angular frequency was swept from 0.1~100 rad/s.

Compression test: To measure the compression properties of hydrogels, we used a universal testing machine (Shimadzu AGS-X10KN, Kyoto, Japan) to conduct compression tests on SFMA/HAMA hydrogels with different HAMA concentrations. Hydrogel samples with a diameter of 9 mm and mean height of 6 mm were measured with a strain rate of 5 mm/min.

Degradation in vitro: To simulate human body fluids, the SFMA and SFMA/HAMA hydrogels were immersed in PBS solution (pH=7.4) with or without lysozyme (1000 U/mL). Then, the hydrogel was placed on a constant temperature shaker at 37°C, and the stirring speed was 60 rpm. After a defined degradation time, the hydrogel samples were removed and washed with deionized water three times, followed by vacuum-drying. The degradation ratio of the swelling ratio was as follows:

$$\text{Degradation ratio } (\%)=M_t/M_0 \times 100$$

Where M_0 is the mass of the initial hydrogel after lyophilization and M_t is the mass of the degraded hydrogel after lyophilization at time t.

Release of Ag^+ ions: Inductively coupled plasma-mass spectrometry (ICP-MS) was used to quantify the release of Ag^+ ions from the SFMA/HAMA/Ag@MOF hydrogel. Briefly, SFMA/HAMA/Ag@MOF hydrogel was incubated in 10 mL PBS solution (pH=7.4). At different time points, PBS supernatant liquor was collected and completely refreshed with fresh PBS. Finally, the collected samples were digested with concentrated nitric acid (HNO_3) to determine Ag^+ iron levels.

Release of EGF: ELISA methods were used to quantify the release of EGF from the SFMA/HAMA/Ag@MOF/PRP hydrogel. Briefly, the hydrogel was incubated in 1 mL PBS solution (pH=7.4). At different time points, 1 mL of fresh PBS was added after removing 1 mL of PBS supernatant liquor from the well. The collected samples were measured by an EGF Human ELISA kit (Meimian, Jiangsu, China), and the accumulative release profiles of EGF were plotted against time.

In vitro antibacterial activity: E. coli and *S. aureus* were utilized to evaluate the antibacterial performance of hydrogels. Each hydrogel sample (600 μL) was placed in 24-well plates, and then 1.5 mL bacterial suspensions with a concentration of 1×10^8 CFU/mL were added. SFMA/HAMA hydrogel was used as a blank control group. After 4 h of incubation at 37°C, serial 10-fold dilutions of the mixture were cultured in Luria-Bertani agar using the pour plate method to count low colony-forming units. The antibacterial ratio of the swelling ratio was as follows:

$$\text{Antibacterial ratio } (\%)=(C_b-C_s)/C_b \times 100$$

Where C_b is the number of culture colonies in the blank control and C_S is the number of culture colonies in the SFMA/HAMA/Ag@MOF hydrogel.

In vitro biocompatibility test

Biocompatibility test: Cell Counting Kit-8 reagent was used to assay cell viability. The 500 μL hydrogel samples were added to a 24-well plate and then irradiated with 405 nm light for 30 s. Next, the 3T3 cell suspension was seeded in a 24-well plate with 20,000 cells in each well. The medium was also changed every two days, and the cells were cultured for 24 h, 48 h and 72 h. Cell viability was tested with CCK-8 by adding CCK-8 solution to each well. The absorbance value was measured by a microplate reader (SH1000, Corona, Japan) at 450 nm.

Live/dead staining: The hydrogels loaded with cells were washed with PBS twice, and then 200 μL of the prepared working solution (2 μM calcein-AM and 8 μM propidium iodide) was added. After 15 min of incubation while being protected from light, stained samples were placed in the well plate under fluorescence microscopy (Olympus BX51, Tokyo, Japan) for observation.

Flow cytometric analysis of apoptosis: Apoptotic cells were detected using an Annexin V-FITC/PI Apoptosis Detection kit (Kaiji Biotech, Nanjing,

China). Briefly, cells were collected by centrifugation at 1,000 × g for 5 min at room temperature. Cells were stained with 5 μL Annexin V-FITC and 10 μL PI for 15 min in the dark. Subsequently, the percentage of apoptotic cells was immediately detected using a NovoCyte flow cytometer (Coulter Epics XL, Beckman, USA) and analyzed using FlowJo software.

Cell migration test: The migration behavior of HUVECs was observed by scratch test *in vitro*. HUVECs were inoculated into 24-well plates (5×10^5 cells/well) and cultured at 37°C for 24 h to form a monolayer of cells. A 200 μl pipette tip was used to make a horizontal scratch, and the cells were gently rinsed with PBS to remove suspended cells and cell fragments. The hydrogel extract solution was added and cultured at 37°C. At the scheduled time, the cells were photographed using a microscope, and the scratch area was measured using Image software. The cell migration rate was calculated based on the following formula:

$$\text{Cell migration (\%)} = \frac{(A_0 - A_t)}{A_0} \times 100\%$$

Where A_0 is the initial scratch area and A_t is the area at different times.

Establishment of a rat wound infection model

Animal experiments were approved by the Institution Animal Ethics Committee of Ruige Biotechnology. Sprague-Dawley (SD) rats (200-220 g) were selected and divided into four groups: the control group, SFMA/HAMA and SFMA/HAMA/Ag@MOF hydrogel groups, and SFMA/HAMA/PRP/Ag@MOF hydrogel group. The rats were anesthetized by intraperitoneal injection of 1% pentobarbital sodium solution at a dose of 65 mg/kg, and the hair on the back of the rats was removed with an electric razor and hair removal cream under anesthesia. Four round wounds with a diameter of 12 mm were made on the back of each rat with a biopsy punch, and then 40 μL mixed bacterial solution (1×10^8 CFU/mL E. coli and 1×10^8 CFU/mL S. aureus) was added to the wound surface. Finally, the hydrogel was covered with the wound surface, and the hydrogel was fixed on the backs of rats with a 15 mm × 15 mm medical PU membrane. The wound dressing was changed every 3 days.

Histological analysis

On the 3rd, 7th and 14th days, one rat in each group was killed, and the wound and its adjacent skin were collected for histological analysis. The wound skin tissues of rats in different groups were fixed in tissue fixation solution for 24 h and then embedded in paraffin wax. The tissue samples were cut longitudinally into 4 μm thick sections, and the tissue sections were stained with hematoxylin and eosin (H&E) and Masson. Finally, all slices were photographed and analyzed by optical microscopy.

Statistical analysis

Statistical analyses were performed using SPSS22.0. All values were tested to be in accordance with a normal distribution, expressed as the means ± SD (standard deviation) from a minimum of three experiments. One-way analysis of variance (ANOVA) was used for comparison between the experiment group and control group. All results were considered statistically significant at $^*P < 0.05$, $^{**}P < 0.01$, $^{***}P < 0.001$.

Results

Characterization of polymers and hydrogels

^{1}H-NMR was used to verify the chemical structure of SFMA and HAMA. As shown in **Figure 1A**, after GMA modification of SF, a new signal peak appears at 6.11 ppm, which is the signal generated by the vibration of H nuclei in -C=CH. Meanwhile, an obvious methyl (-CH_3) signal appears at 1.89 ppm. Therefore, we can confirm that the ethynyl group can be successfully modified on SF molecules using GMA under the current experimental conditions [36]. As shown in **Figure 1B**, it was found that the pure HA after modification had obvious chemical signals of -C=CH at chemical displacements of 5.84 ppm and 6.26 ppm [32]. TEM images of MOF@Ag showed spherical nanoparticles with sizes ranging from 80 to 120 nm (**Figure 1C**). When the irradiation time reached 60 s, the solution had lost its fluidity, and obvious gel blocks were formed at the bottom of the glass bottle, which indicated that the solution had completely realized sol-gel transformation (**Figure 1D**).

Hydrogels have interpenetrating porous structures with pore sizes usually larger than indi-

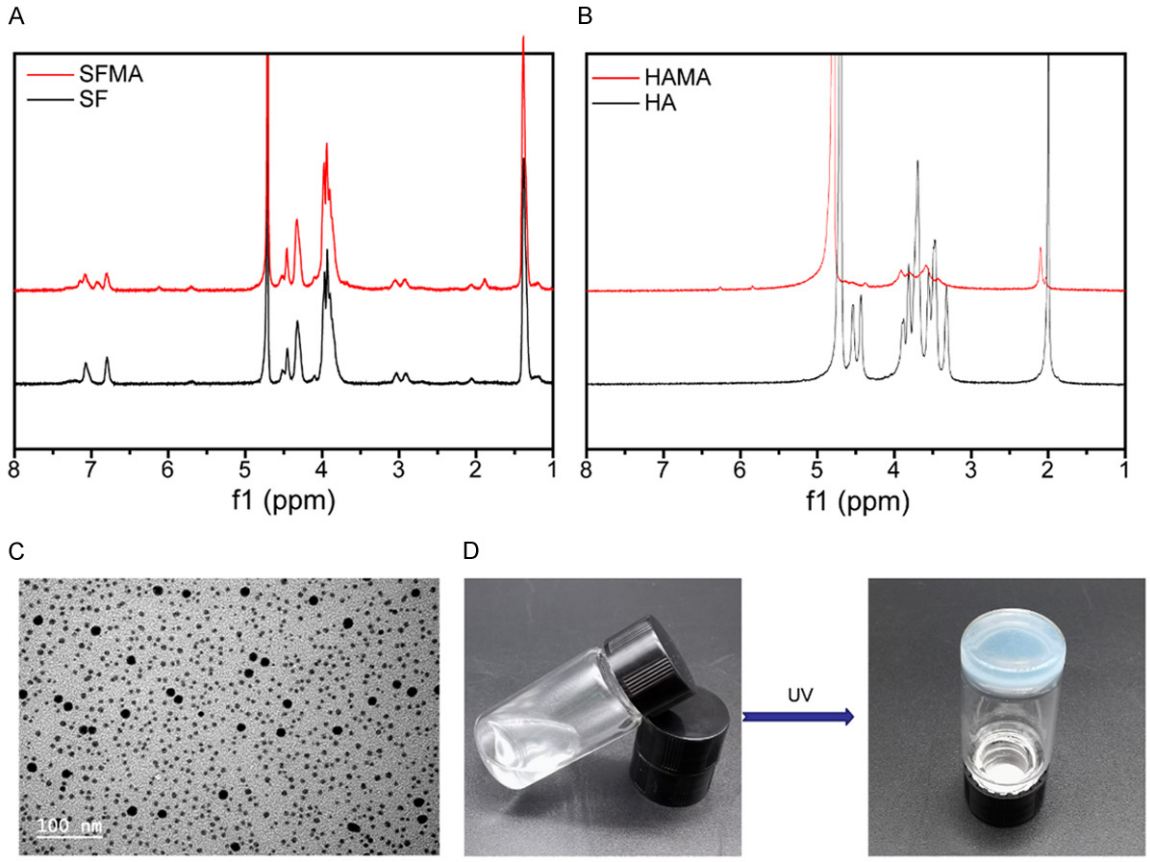

Figure 1. A. ^{1}H NMR spectra of SF and SFMA. B. ^{1}H NMR spectra of HA and HAMA. C. TEM images of Ag@MOF. D. Photograph of the SFMA/HAMA hydrogel through UV crosslinking.

vidual cells. In addition, hydrogels contain a large number of hydrophilic groups, which easily absorb water and swell, similar to the natural extracellular matrix (EMC). As shown in **Figure 2A**, all hydrogels exhibited interpenetrating porous microstructures, which could affect the swelling rate, mechanical properties and drug delivery of hydrogels. The interconnected porous structure of hydrogels creates a 3D microenvironment supporting cell proliferation, migration and intercellular interactions [37]. When used as a medical dressing, it can keep the wound surface moist and facilitate the growth of new granulation tissue without causing secondary injury [38].

Rheological properties

As shown in **Figure 2B**, all the storage moduli (G') of hydrogels were higher than the loss modulus (G"), which indicated a completely gelled network material. Meanwhile, the G' of the SFMA/HAMA hydrogel increased with increasing HA concentration, which indicated an increase in the crosslinking density in the hydrogel. As shown in **Figure 2C**, the G' was approximately one order of magnitude higher than the G" over the frequency sweep (0.1-10 Hz), indicating a predominant elastic response.

Swelling ratio analysis

When human skin is injured, a large amount of fluid will exude from the wound, which easily causes pathogenic microorganism infection, leading to delayed healing or chronic nonhealing wounds. In clinical medicine, medical dressings are required not only to absorb excessive exudate but also to maintain a moist wound healing microenvironment to promote wound healing. Thus, good swelling performance is an important index to evaluate the comprehensive performance of medical dressings. The swelling property is always the unique property of the hydrogel, which represents the water absorption performance of the hydro-

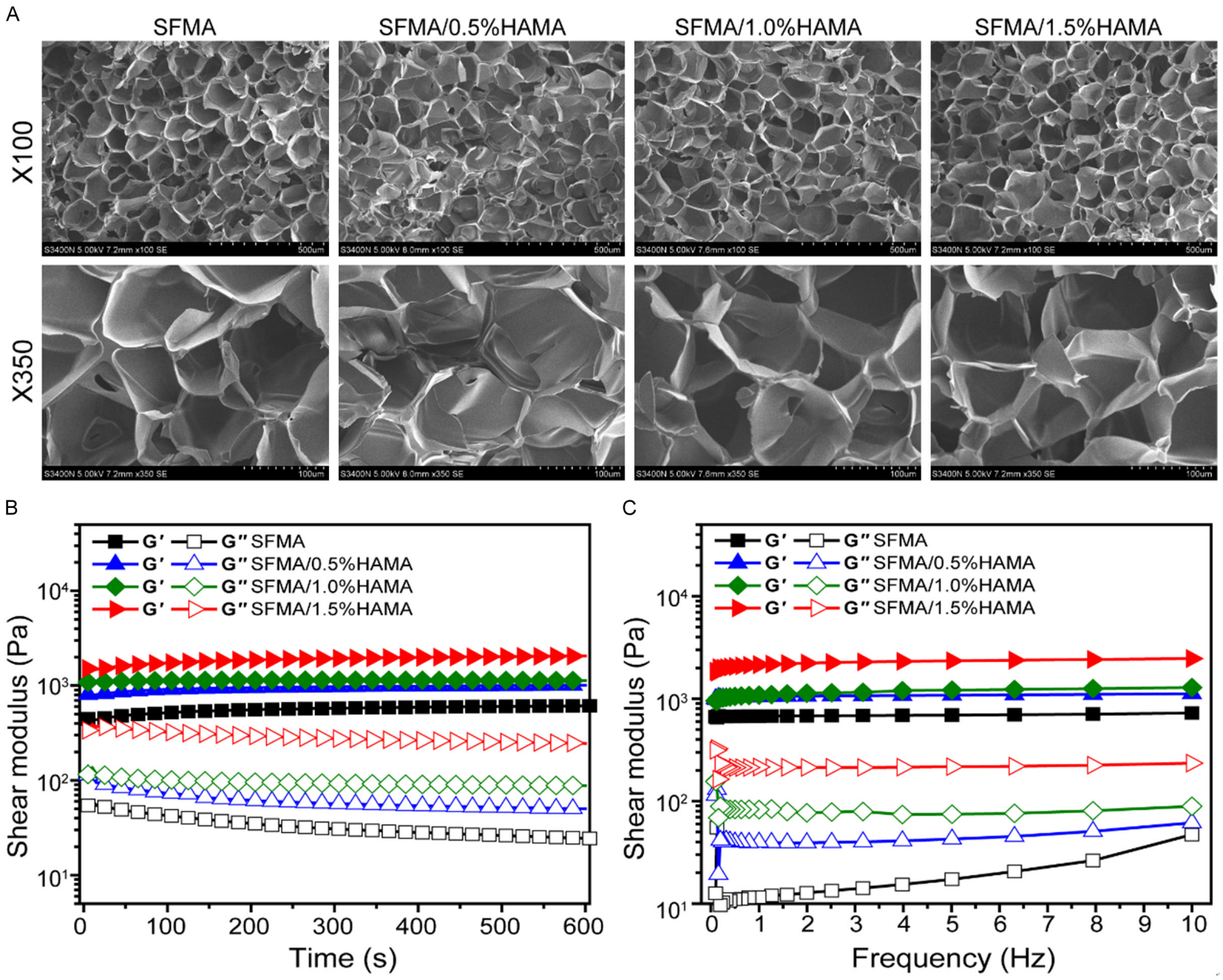
A
SFMA
SFMA/0.5%HAMA
SFMA/1.0%HAMA
SFMA/1.5%HAMA
X100
X350
B
G′ G″ SFMA
G′ G″ SFMA/0.5%HAMA
G′ G″ SFMA/1.0%HAMA
G′ G″ SFMA/1.5%HAMA
Shear modulus (Pa)
Time (s)
C
Shear modulus (Pa)
Frequency (Hz)

Figure 2. A. SEM images of SFMA/HAMA hydrogels with different HAMA concentrations. B. Rheological properties of hydrogels. C. The viscosity of hydrogels within the frequency range of 0.1-10 Hz.

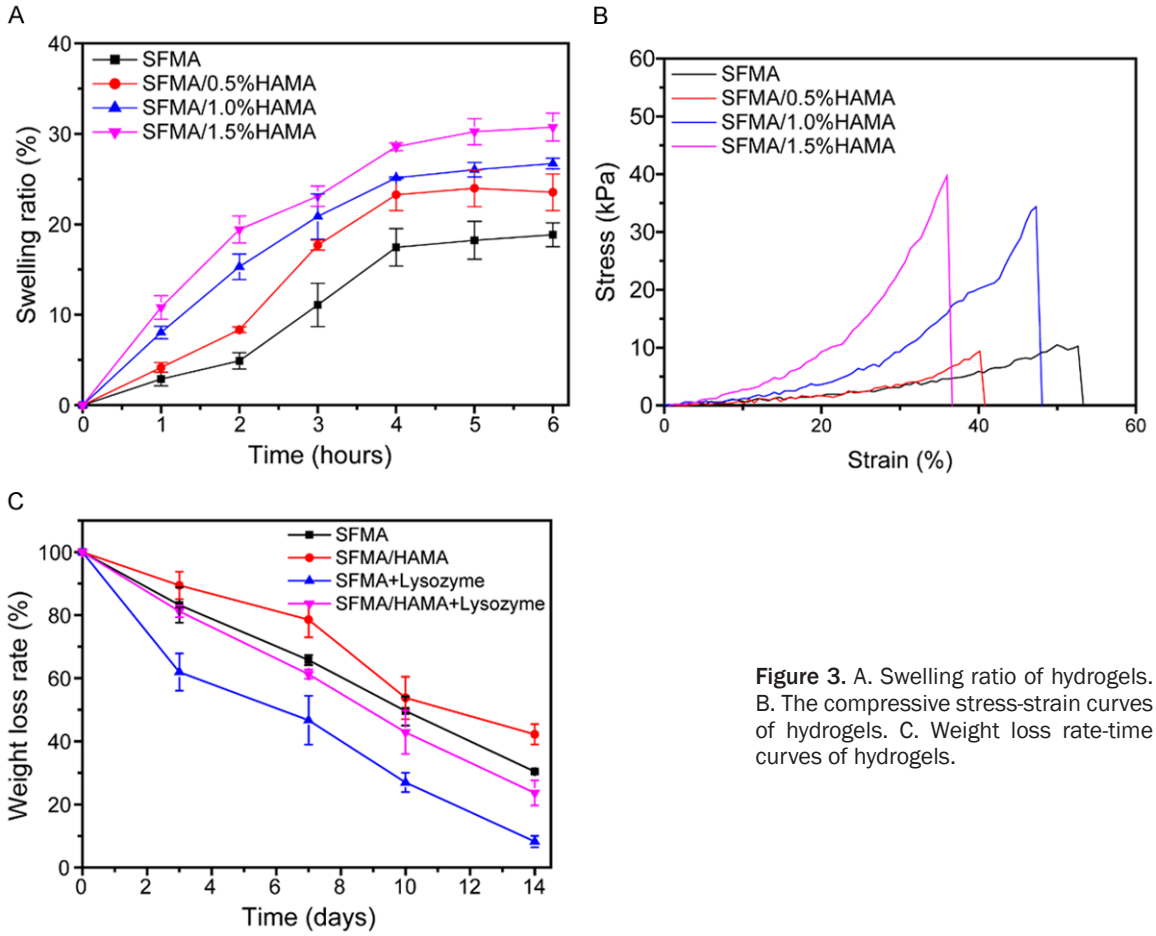

Figure 3. A. Swelling ratio of hydrogels. B. The compressive stress-strain curves of hydrogels. C. Weight loss rate-time curves of hydrogels.

gel. A higher swelling ratio indicates a stronger water absorption performance. The swelling property of the hydrogel also affects the sustained release rate of the drug. Wound infection will have many exudates; traditional dressings have poor water absorption and cannot absorb water continuously [39]. Hydrogels have continuous water absorption during a certain period of time to ensure that the exudation of the wound can be steadily absorbed [40, 41].

As shown in **Figure 3A**, the swelling rate of all hydrogels showed trapezoidal growth, indicating that the swelling rate of the hydrogel no longer increased after the initial water absorption rate reached a certain limit. Meanwhile, all hydrogels reached their swelling equilibrium state in the first 4 h. The swelling rate of the SFMA/1.5% HAMA hydrogel showed a maximum swelling ratio of 30%, and the swelling ratio of the SFMA/HAMA hydrogel increased gradually with increasing HA concentration.

Compression analysis

Stress-strain curve of SFMA/HAMA hydrogels with different HAMA concentrations. As shown in **Figure 3B**, the compression strength of the SFMA/1.0% HAMA and SFMA/1.5% HAMA hydrogels was much greater than that of the SFMA and SFMA/0.5% HAMA hydrogels. This was because the SFMA/1.0% HAMA and SFMA/1.5% HAMA hydrogels have more cross-linking points to form, thus forming a high-density network. Moreover, friction between polymer chains increased in tight structures. When the hydrogel was compressed, the polymer chain was constrained to achieve different

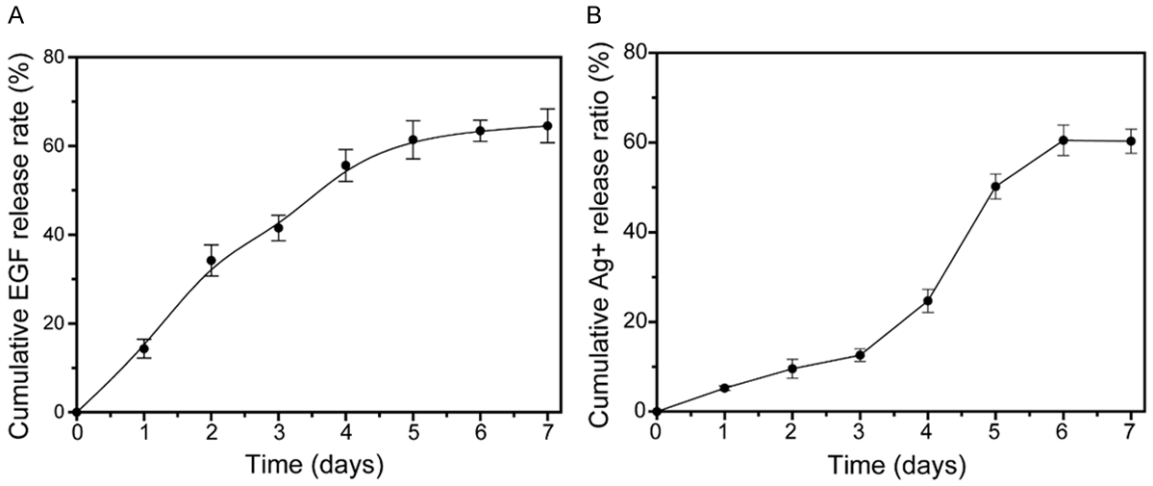

Figure 4. A. *In vitro* release curves of EGF. B. *In vitro* release curves of Ag^+.

deformations, requiring more force. All results indicated that the increase in HAMA concentration was beneficial to enhance the mechanical properties of SFMA/HAMA hydrogels. In summary, the SFMA/1.0% HAMA hydrogel was selected as the best hydrogel for the next application.

In vitro degradation

The degradation of biomaterials is an important problem in tissue engineering applications [42]. Ideally, the degradation rate of biomaterials should be regulated according to the regeneration process of implanted tissue, thus guiding the formation of new tissue. Complex enzymatic pathways lead to the degradation of biomaterials when exposed to body fluids, so in vitro enzymatic degradation is an ideal choice to better predict the stability of biomaterials *in vivo*. As shown in **Figure 3C**, all hydrogels degraded gradually over time. Meanwhile, the hydrogel degraded faster with the enzyme. In the degradation process, the pure SFMA hydrogel degraded more than 90% at 14 days. After HAMA was added, the degradation performance of biomaterials was improved, and the degradation was nearly 70% at 14 days. Generally, animal wound healing time is approximately 14-21 days, so biomaterials should also have an appropriate degradation time to match the rate of skin regeneration. *In vitro* degradation experiments showed that the SFMA/HAMA hydrogel was suitable for wound repair.

Ag^+ release and EGF studies in vitro

Figure 4A and **4B** show the cumulative slow-release curves of Ag^+ ions and EGF in the hydrogel, and the release kinetics remained controlled through day 7. The cumulative release curve of EGF showed slow release in the first 4 days and then maintained a relatively slow release rate. The main reason for the slow release was the swelling and degradation of the hydrogel. The cumulative release curve of Ag^+ ions showed a slow release trend during the first 3 days and then maintained the trend of quick release. This was mainly because elemental Ag existed in Ag@MOF nanoparticles in the early stage, and then the elemental Ag gradually hydrolyzed to form Ag^+ ions.

In vitro antibacterial evaluation

Wound infection is a major challenge in wound care management, and hydrogel dressings with antibacterial properties can avoid wound infection and maintain proper moisture around the wound. Gram-positive *S. aureus* and gram-negative *E. coli* were used as representative pathogens in skin infection to evaluate the antibacterial performance of the as-prepared hydrogel in this study. As shown in **Figure 5A**, after coincubation with SFMA/HAMA/PRP/Ag@MOF hydrogel at 37°C for 4 h, colonies of surviving *E. coli* and *S. aureus* on agar plates of the SFMA/HAMA/PRP/Ag@MOF(10) and SFMA/HAMA/PRP/Ag@MOF(20) hydrogel treatment groups were significantly lower than those of the SFMA/HAMA/PRP hydrogel group. As

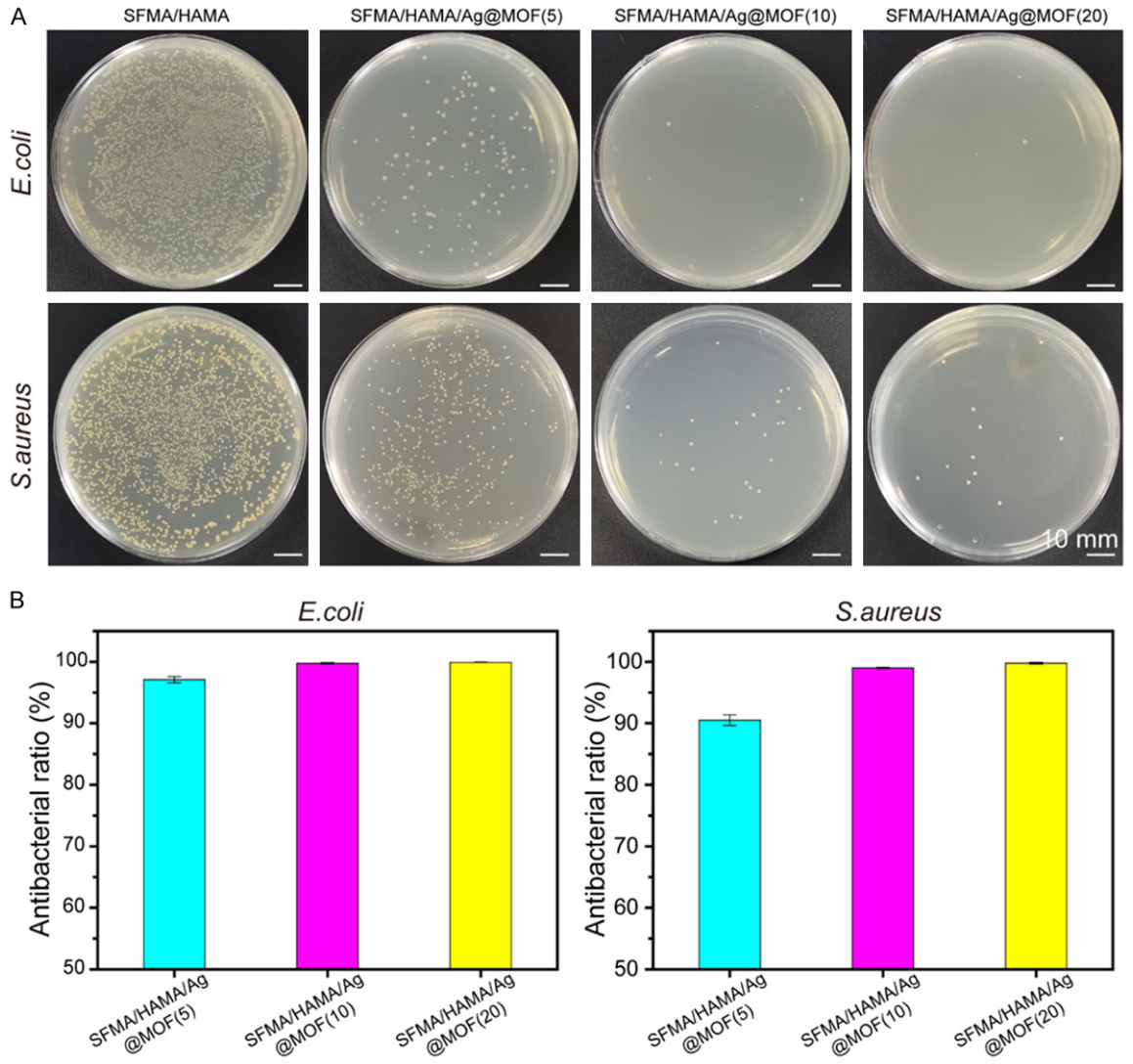

Figure 5. A. Images of E. coli and S. aureus colonies after coculture with SFMA/HAMA/PRP hydrogels with different Ag@MOF concentrations. B. Antibacterial rate of *E. coli* and *S. aureus*.

shown in **Figure 5B**, the antibacterial ratios of SFMA/HAMA/PRP/Ag@MOF(5), SFMA/HAMA/PRP/Ag@MOF(10) and SFMA/HAMA/PRP/Ag@MOF(20) hydrogels against *E. coli* and *S. aureus* were 97.1 ± 0.5%, 90.5 ± 0.9%, 99.8 ± 0.1%, 99.0 ± 0.1%, 99.9 ± 0.1%, and 99.8 ± 0.2%, respectively. When the concentration of Ag@MOF reached 10 μg/mL, the antibacterial ratio of SFMA/HAMA/PRP/Ag@MOF demonstrated a better antibacterial activity with an antibacterial ratio of > 95%. Prior studies reported that Ag@MOF displayed an antibacterial effect by releasing silver ions and inducing the generation of reactive oxygen species (ROS) [20]. Moreover, the low concentration of Ag^+ ions helps to reduce the cytotoxicity to cell tissue. Considering the antibacterial activity and biocompatibility, 10 μg/mL Ag@MOF was selected as the optimal concentration.

Biocompatibility of the hydrogels

Medical dressings are products that come into direct contact with tissue cells on the wound surface and must be nonirritating, nontoxic and nonsensitizing to the human body [43]. Therefore, the evaluation of the biocompatibility of materials is essential in the research and design of biomedical materials. NIH-3T3 fibroblasts for this assay because they play an integral role in the process of wound healing.

Figure 6A shows a fluorescence microscope photograph of 3T3 cells cocultured on the hydrogel surface for 1, 2 and 3 days. The green color represents viable cells; red color represents dead cells. As the coculture time increased, the density of 3T3 cells gradually increased. Meanwhile, the SFMA/HAMA/PRP hydrogel group showed the highest cell density. Furthermore, quantitative analysis of cell proliferation measured by CCK-8 assay also verified the same phenomenon that SFMA/HAMA/PRP and SFMA/HAMA/PRP/Ag@MOF had high cell viability (**Figure 6B**). All results indicated that the SFMA/HAMA/PRP/Ag@MOF hydrogel has good biocompatibility and can promote cell proliferation.

As shown in **Figure 6C** and **6D**, the staining of dead cells and living cells showed that there was no significant difference between early apoptotic cells and necrotic cells among the three groups, which indicated that the hydrogel did not increase apoptosis. On the other hand, the results of the cell cycle analysis showed that the percentages of cells in G0/G1 phase and S phase were similar in the three groups. The above results show that the hydrogel has good biocompatibility with cells.

To further study the effect of the hydrogel on the proliferation of HUVECs, we carried out scratch experiments *in vitro*. HUVECs in all groups moved to the scratches (**Figure 6E**). Compared with the control group, the cell migration rate of the PRP group and hydrogel group increased by approximately 30.83% within 8 h (**Figure 6F**).

Among them, Ag@MOF and SFMA/HAMA had no significant effect on cell migration. The scratches in the PRP group and the hydrogel group almost disappeared after 24 h, which indicated that SFMA/HAMA/PRP/Ag@MOF hydrogel could accelerate HUVEC migration. Prior studies have also revealed that PRP can promote cell migration [44].

Evaluation of wound healing in vivo

The wound repair effect of the SFMA/HAMA/PRP/Ag@MOF hydrogel was evaluated by establishing an infected wound model in rats. The results of the appearance photos of the wound showed that the wound treated with SFMA/HAMA/PRP/Ag@MOF hydrogel was much more efficient than the other three groups (**Figure 7A**). On the 3rd day, obvious secretions and pus were seen in the control group, and the wound area did not decrease significantly. Meanwhile, the wound area decreased to a certain extent in the SFMA/HAMA and SFMA/HAMA/Ag@MOF hydrogel groups, while the wound contraction area was the largest in the SFMA/HAMA/PRP/Ag@MOF hydrogel group, indicating that it played a relatively good role in promoting wound healing. On the 7th and 10th days, the effect of the three hydrogel groups was better than that of the control group. On the 14th day, although all groups showed a very small residual wound area, the SFMA/HAMA/PRP/Ag@MOF hydrogel group had the least scarring. The quantitative analysis of the wound healing rate showed that 7 days after the operation, the wound closure rate of the SFMA/HAMA/PRP/Ag@MOF hydrogel group (84.1%) was significantly higher than that of the control group (78.2%), SFMA/HAMA/hydrogel group (80.1%) and SFMA/HAMA/Ag@MOF hydrogel group (81.5%) (**Figure 7B**). All results showed that SFMA/HAMA/PRP/Ag@MOF hydrogel treatment had better healing performance in the early healing stage. In conclusion, the SFMA/HAMA/PRP/Ag@MOF hydrogel group had a better wound healing effect than the control group and SFMA/HAMA group, which was attributed to the antibacterial properties of the hydrogel, the ideal biocompatibility of silk fibroin, hyaluronic acid and PRP in promoting wound healing, and the excellent wound repair environment provided by the hydrogel.

Histological evaluation

Wound healing is a complex and orderly process involving hemostasis, inflammation, proliferation, and tissue remodeling [45]. On the 3rd day, all groups showed significant acute inflammation (**Figure 7C**), which may be caused by bacterial infection and inflammatory cell migration. In addition, compared with the control group, obvious epithelialization of skin tissue was observed in the SFMA/HAMA/Ag@MOF and SFMA/HAMA/PRP/Ag@MOF hydrogel groups. On the 7th day, due to the short recovery time, the wounds of the four groups showed larger inflammatory areas, and the wounds treated with SFMA/HAMA/Ag@MOF and SFMA/HAMA/PRP/Ag@MOF hydrogels had

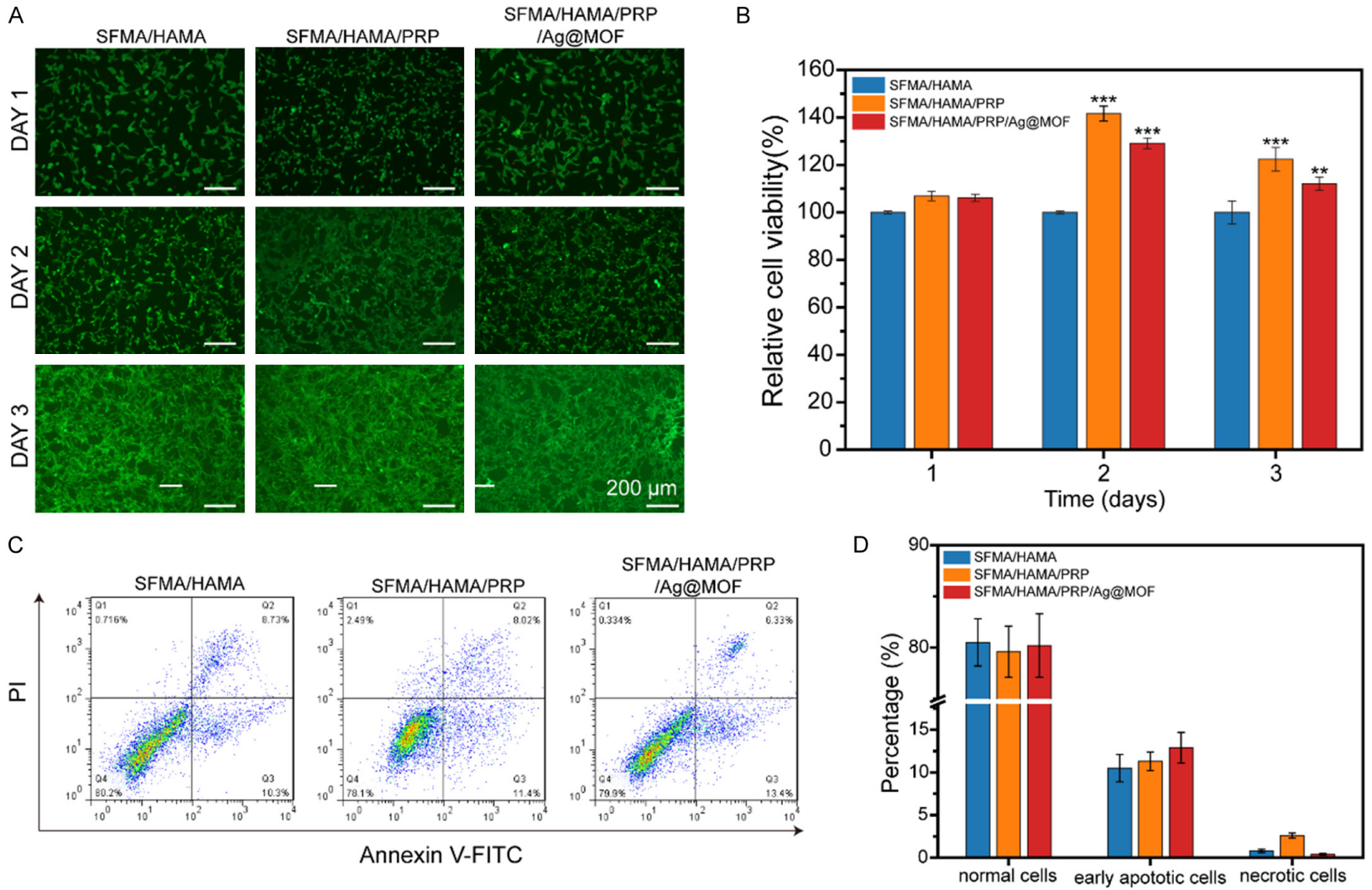
A
SFMA/HAMA
SFMA/HAMA/PRP
SFMA/HAMA/PRP /Ag@MOF
DAY 1
DAY 2
DAY 3
200 μm
B
Relative cell viability(%)
Time (days)
SFMA/HAMA
SFMA/HAMA/PRP
SFMA/HAMA/PRP/Ag@MOF
***
***
***
**
C
SFMA/HAMA
SFMA/HAMA/PRP
SFMA/HAMA/PRP /Ag@MOF
PI
Annexin V-FITC
Q1 0.716%
Q2 8.73%
Q4 80.2%
Q3 10.3%
Q1 2.49%
Q2 8.02%
Q4 78.1%
Q3 11.4%
Q1 0.334%
Q2 6.33%
Q4 79.9%
Q3 13.4%
D
Percentage (%)
SFMA/HAMA
SFMA/HAMA/PRP
SFMA/HAMA/PRP/Ag@MOF
normal cells
early apototic cells
necrotic cells

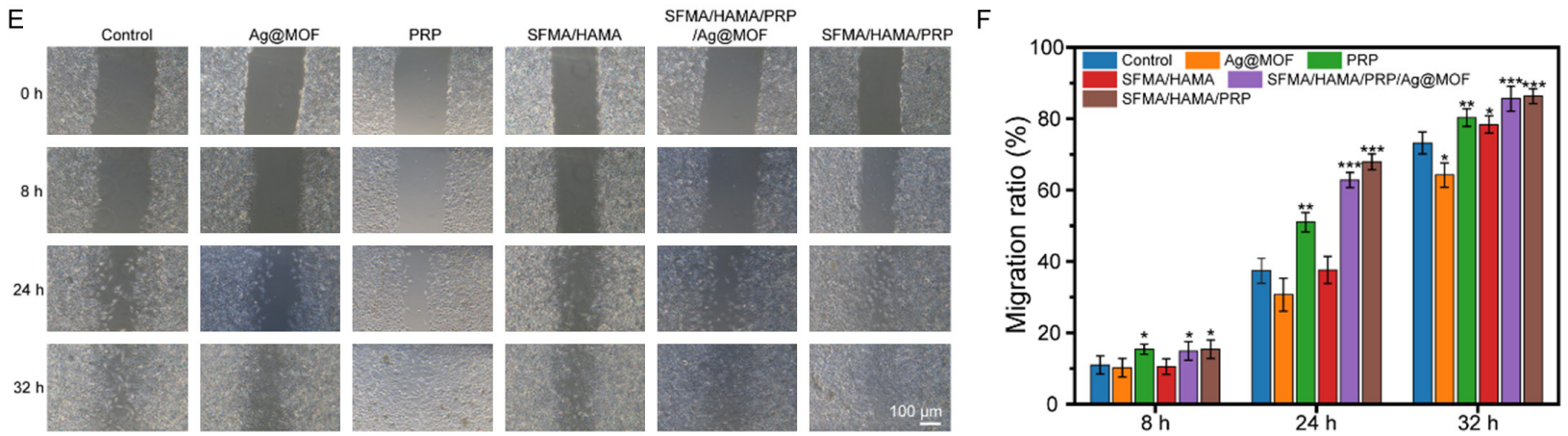

Figure 6. A. Live-dead staining of HSF cells cultured on the SFMA/HAMA, SFMA/HAMA/PRP and SFMA/HAMA/PRP/Ag@MOF hydrogels at days 1, 2 and 3. B. Cell viabilities of HSF cells treated with various hydrogels. C. Flow cytometric analysis results of apoptosis. D. The apoptosis rate of cells was detected by flow cytometry. E. Representative images of the scratch assay. F. Statistical analysis of the scratch assay.

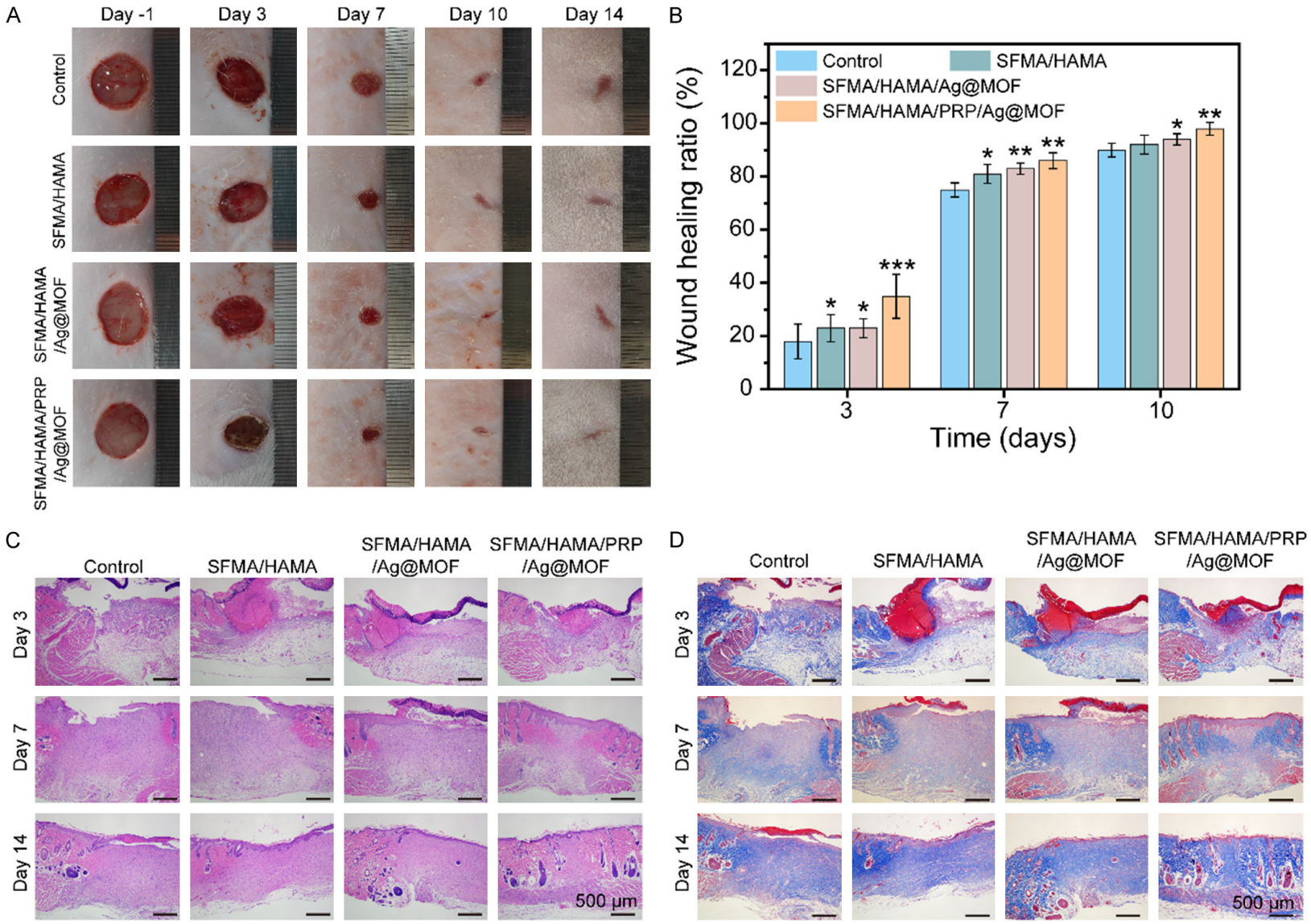

Figure 7. A. Images of wounds at different time points. B. The healing ratio rate. C. Representative H&E staining of skin tissue sections at 3, 7 and 14 days. D. Representative Masson staining of skin tissue sections at 3, 7 and 14 days.

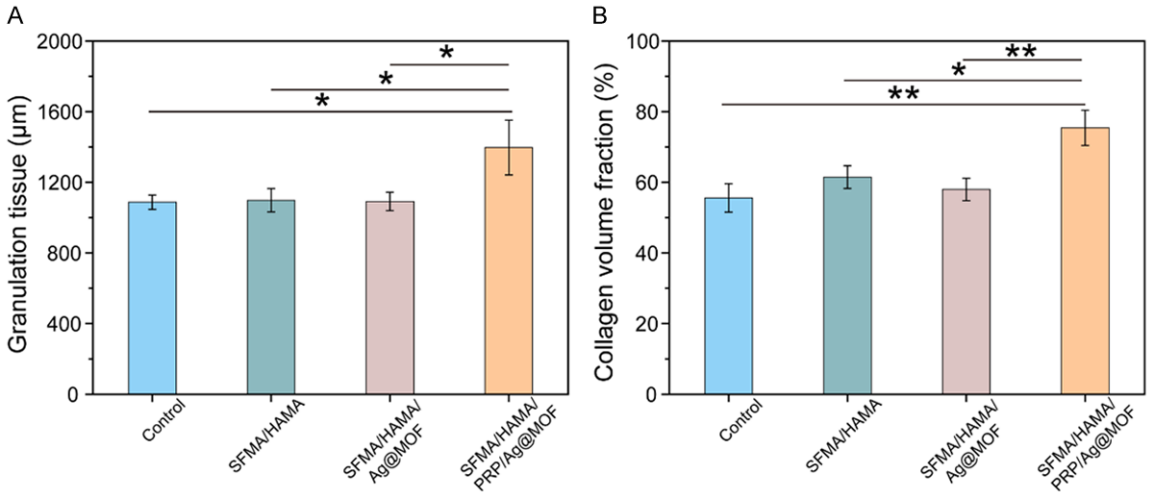

Figure 8. A. Quantitative analysis of the granulation tissue thickness and the collagen volume fraction of different groups for 14 days. B. Quantitative analysis of the collagen volume fraction of different groups for 14 days.

less inflammatory cell infiltration than the control group and SFMA/HAMA hydrogel group, indicating that SFMA/HAMA/Ag@MOF and SFMA/HAMA/PRP/Ag@MOF hydrogels could reduce the inflammatory reaction of the wound at the initial stage of wound healing. It is worth noting that the control group has the lowest proportion of extracellular matrix, which also means that the granulation tissue of the control group grows the slowest, which fully reflects the role of hydrogel in promoting wound healing and once again proves the correctness of the theory of wet healing. Subsequently, on the 14 h day, the inflammatory reaction of the wound site in all groups significantly subsided compared with the 7 days after operation, indicating that the wounds of the four groups had transitioned from the inflammatory phase to the proliferative phase. However, there was still a significant gap in the area of inflammation among the four groups; that is, the control group had the largest inflammatory area, while the SFMA/HAMA/PRP/Ag@MOF hydrogel group had the smallest inflammatory area. In addition, some skin appendages, such as hair follicles and sweat glands, were clearly observed in the wound site of the SFMA/HAMA/PRP/Ag@MOF hydrogel group, while these skin appendages were rarely or even absent in the other groups. As shown in **Figure 8A**, there is a significant difference in the thickness of granulation tissue between the SFMA/HAMA/PRP/Ag@MOF group and other groups, reaching 1397 μm. Meanwhile, the collagen content reached 75.41%, which was significantly different from the control group and other hydrogel groups (**Figure 8B**). These results show that the SFMA/HAMA/PRP/Ag@MOF hydrogel can promote wound healing. These results suggest that the synergistic effect of Ag@MOF and PRP in the SFMA/HAMA/PRP/Ag@MOF hydrogel can promote the epithelialization of infected wound tissue and reduce inflammation.

Collagen is an important component of the extracellular matrix and plays an important role in the function of skin tissue [46]. Masson staining was used to investigate collagen deposition in the wound at different healing times (**Figure 7D**). Compared with the collagen deposition at 14 days, the overall collagen deposition at the wound site was relatively low at the initial stage of wound healing (3 days). The reason was that the wound was mainly in the inflammatory reaction stage after 3 days, and relatively few fibroblasts infiltrated the wound site. On the 14th day, wound healing was in the stage of proliferation and remodeling, when the number of fibroblasts increased and collagen synthesis and deposition increased significantly, so Masson staining showed a dark green color. Generally, the overall trends at 3 days and 14 days were consistent. Compared with the blank group and SFMA/HAMA hydrogel group, more collagen was deposited in the wounds treated with SFMA/HAMA/Ag@MOF and SFMA/HAMA/PRP/Ag@MOF hydrogels, and the collagen fibers were most evenly distributed in

the wounds treated with SFMA/HAMA/PRP/Ag@MOF hydrogels.

Through the analysis of the materials, we concluded that SFMA/HAMA/PRP/Ag@MOF hydrogel as a wound dressing has a good function to promote the healing of infected wounds. The reasons can be attributed to the following points. First, SFMA/HAMA/PRP/Ag@MOF hydrogel can quickly absorb blood and tissue secretions into the hydrogel because of its unique porous structure, which will help to enhance wound healing [47]. Second, SFMA/HAMA/PRP/Ag@MOF hydrogels can slowly release growth factor (EGF), and EGF can promote metaplastic ductal formation in the process of tissue regeneration [48]. Third, the SFMA/HAMA/PRP/Ag@MOF hydrogel has excellent antibacterial properties, which can reduce wound infection by either inhibiting or killing the bacteria [49], thus improving the speed of wound healing.

Discussion

Delayed or even non healing of wounds remains a major clinical challenge so far [50]. Generally, wound healing includes four stages: hemostasis, inflammation, proliferation, and tissue remodeling [51]. With the in-depth study of wound healing mechanism and the accumulation of wound treatment experience, the importance of clinical treatment of trauma and microenvironment has attracted more and more attention. A lot of evidence shows that the treatment plan cannot be completed in a wound that is not fully debridement and is not conducive to tissue repair in the microenvironment [52]. In addition to debridement, trauma treatment also requires controlling infection, inflammation, and regulating water balance. Therefore, if the wound is to be repaired well, it must be free of infection and excessive exudate, and it needs a microenvironment conducive to tissue growth and vascularization. This puts forward specific requirements and necessary conditions for the design of tissue engineering wound repair materials. However, most of the reported wound repair materials currently have shortcomings and single performance, which cannot meet the needs of various stages of wound healing at the same time.

The reason why SFMA/HAMA/PRP/Ag@MOF hydrogel has a good healing promoting effect is: Firstly, SFMA/HAMA/PRP/Ag@MOF can absorb some of the wound exudate without the need for debridement treatment in the early stage, thus creating a good physiological environment for the wound. Absorbing the wound exudate not only stores nutrients for wound healing but also maintains a moist environment for a long time. A humid and hypoxic environment can maintain a normal potential gradient from the edge of the wound to the center, stimulating the generation of capillaries [53]. Secondly, SFMA/HAMA/PRP/Ag@MOF hydrogel slowly releases a variety of cytokines, and activates cell surface receptors in the wound through Erk-Akt signaling pathway and Yes associated protein (YAP) to regulate gene expression, thus regulating cell proliferation and differentiation, and participating in the degradation of matrix in the wound and tissue reconstruction [54]. In addition, these growth factors can promote angiogenesis in the wound, provide blood supply and abundant nutrients for wound repair, and alleviate neuropathic scar pain at the wound site [55].

Additionally, SFMA/HAMA/PRP/Ag@MOF has excellent antibacterial properties, slow release of Ag^+, and reduced cytotoxicity to tissues. Early bacterial infections in wounds can increase exudate and delay wound healing, while SFMA/HAMA/PRP/Ag@MOF persistent antibacterial activity creates a sterile microenvironment for the wound, which can reduce the invasion of pathogens and the inflammatory reaction at the wound site, thus promoting wound healing. Furthermore, SFMA/HAMA/PRP/Ag@MOF hydrogel has a through porous structure, which not only supports the formation of granulation tissue at the initial stage, but also helps the adhesion and migration of fibroblasts and endothelial cells, and provides necessary space for the formation of new blood vessels [56]. In addition, with the degradation of hydrogel scaffold, its degradation products provide essential nutrients for the formation of granulation tissue. The growth of granulation tissue is also an important link in the process of wound repair. Granulation tissue is composed of fibroblasts, endothelial cells, and new capillaries, which helps to fill the tissue defect of the wound, helps to contract the wound, and creates necessary conditions for the crawling of epithelial cells [57].

In summary, SFMA/HAMA/PRP/Ag@MOF combines the dual functions of medical dressings and tissue engineering scaffold materials, which have a high fluid absorption rate, and durable inherent antibacterial ability. In addition, it creates a moist, sterile and closed microenvironment for the wound, reduces the invasion of pathogens and inflammatory reaction of the wound site, and can control and absorb wound exudation, and promote the normal growth of granulation and epithelial tissue. The above advantages can fully demonstrate SFMA/HAMA/PRP/Ag@MOF Hydrogel plays a promoting role in four stages of wound healing: hemostasis, inflammation, proliferation and tissue remodeling.

Conclusions

In summary, we successfully prepared Ag@MOF and PRP-loaded SFMA/HAMA hydrogels for wound treatment, particularly for infected wounds. By adjusting the concentration of HAMA, there were good rheological properties, swelling capability, appropriate mechanical properties and controllable biodegradability which make SFMA/HAMA/PRP/Ag@MOF hydrogels highly suitable for their application in medical applications. These released studies indicate that the SFMA/HAMA/PRP/Ag@MOF hydrogel showes sustained release. *In vitro* antibacterial experiments showed that the SFMA/HAMA/Ag@MOF hydrogel had excellent antibacterial properties, and the SFMA/HAMA/PRP/Ag@MOF(10) hydrogel was selected as the best concentration.

The results of CCK8 and live/dead assays indicated that the SFMA/HAMA/PRP/Ag@MOF hydrogel had satisfactory biocompatibility. Finally, the SFMA/HAMA/PRP/Ag@MOF hydrogel has a therapeutic effect on wound healing of infected wounds, including the wound healing rate, inflammatory cell accumulation, epidermis formation and granulation tissue thickness. Overall, our results suggested that the SFMA/HAMA/PRP/Ag@MOF hydrogel has great potential for use as an antimicrobial dressing for accelerating the wound healing process (especially wound infection).

Acknowledgements

This study was supported by the Science and Technology Project of Panyu District (2019Z0425).

Disclosure of conflict of interest

None.

Address correspondence to: Bin Wu, Department of Orthopedics, The Second People's Hospital of Panyu District, Guangzhou 511400, Guangdong, China. E-mail: wubinfff@163.com; Biao Cheng, Department of Burn and Plastic Surgery, General Hospital of Southern Theater Command, PLA, Guangzhou 510010, Guangdong, China. E-mail: chengbiaocheng@163.com

References

[1] Qian S, Wang J, Liu Z, Mao J, Zhao B, Mao X, Zhang L, Cheng L, Zhang Y, Sun X and Cui W. Secretory fluid-aggregated janus electrospun short fiber scaffold for wound healing. Small 2022; 18: e2200799.

[2] Berthiaume F and Hsia HC. Regenerative approaches for chronic wounds. Annu Rev Biomed Eng 2022; 24: 61-83.

[3] Duan G, Wen L, Sun X, Wei Z, Duan R, Zeng J, Cui J, Liu C, Yu Z, Xie X and Gao M. Healing diabetic ulcers with MoO nanodots possessing Intrinsic ROS-scavenging and bacteria-killing capacities. Small 2022; 18: e2107137.

[4] Lisboa FA, Dente CJ, Schobel SA, Khatri V, Potter BK, Kirk AD and Elster EA. Utilizing precision medicine to estimate timing for surgical closure of traumatic extremity wounds. Ann Surg 2019; 270: 535-543.

[5] Kim JH, Kim I, Seol YJ, Ko IK, Yoo JJ, Atala A and Lee SJ. Neural cell integration into 3D bioprinted skeletal muscle constructs accelerates restoration of muscle function. Nat Commun 2020; 11: 1025.

[6] Xue M, Zhao R, Lin H and Jackson C. Delivery systems of current biologicals for the treatment of chronic cutaneous wounds and severe burns. Adv Drug Deliv Rev 2018; 129: 219-241.

[7] Andreadis ST and Geer DJ. Biomimetic approaches to protein and gene delivery for tissue regeneration. Trends Biotechnol 2006; 24: 331-337.

[8] Deng Y, Yang C, Zhu Y, Liu W, Li H, Wang L, Chen W, Wang Z and Wang L. Lamprey-teeth-inspired oriented antibacterial sericin microneedles for infected wound healing improvement. Nano Lett 2022; 22: 2702-2711.

[9] Peng H, Rossetto D, Mansy SS, Jordan MC, Roos KP and Chen IA. Treatment of wound infections in a mouse model using Zn-releasing phage bound to gold nanorods. ACS Nano 2022; 16: 4756-4774.

[10] Bi X, Bai Q, Liang M, Yang D, Li S, Wang L, Liu J, Yu W, Sui N and Zhu Z. Silver peroxide nanopar-

ticles for combined antibacterial sonodynamic and photothermal therapy. Small 2022; 18: e2104160.
[11] Chen CY, Yin H, Chen X, Chen TH, Liu HM, Rao Ss, Tan YJ, Qian YX, Liu YW, Hu XK, Luo MJ, Wang ZX, Liu ZZ, Cao J, He ZH, Wu B, Yue T, Wang YY, Xia K, Luo ZW, Wang Y, Situ WY, Liu WE, Tang SY and Xie H. Ångstrom-scale silver particle-embedded carbomer gel promotes wound healing by inhibiting bacterial colonization and inflammation. Sci Adv 2020; 6: eaba0942.
[12] Alizadehgiashi M, Nemr CR, Chekini M, Pinto Ramos D, Mittal N, Ahmed SU, Khuu N, Kelley SO and Kumacheva E. Multifunctional 3D-printed wound dressings. ACS Nano 2021; 15: 12375-12387.
[13] Qiao Y, He J, Chen W, Yu Y, Li W, Du Z, Xie T, Ye Y, Hua S, Zhong D, Yao K and Zhou M. Light-activatable synergistic therapy of drug-resistant bacteria-infected cutaneous chronic wounds and nonhealing keratitis by cupriferous hollow nanoshells. ACS Nano 2020; 14: 3299-3315.
[14] Cobos M, De-La-Pinta I, Quindós G, Fernández MJ and Fernández MD. Graphene oxide-silver nanoparticle nanohybrids: synthesis, characterization, and antimicrobial properties. Nanomaterials (Basel) 2020; 10: 376.
[15] Zhang G, Liu Y, Gao X and Chen Y. Synthesis of silver nanoparticles and antibacterial property of silk fabrics treated by silver nanoparticles. Nanoscale Res Lett 2014; 9: 216.
[16] Lu J, Xu H, Yu H, Hu X, Xia J, Zhu Y, Wang F, Wu HA, Jiang L and Wang H. Ultrafast rectifying counter-directional transport of proton and metal ions in metal-organic framework-based nanochannels. Sci Adv 2022; 8: eabl5070.
[17] Han Z, Wang K, Min H, Xu J, Shi W and Cheng P. Bifunctionalized metal-organic frameworks for pore-size-dependent enantioselective sensing. Angew Chem Int Ed Engl 2022; 61: e202204066.
[18] Haider G, Usman M, Chen TP, Perumal P, Lu KL and Chen YF. Electrically driven white light emission from intrinsic metal-organic framework. ACS Nano 2016; 10: 8366-8375.
[19] Zhang M, Wang D, Ji N, Lee S, Wang G, Zheng Y, Zhang X, Yang L, Qin Z and Yang Y. Bioinspired design of sericin/chitosan/Ag@MOF/GO hydrogels for efficiently combating resistant bacteria, rapid hemostasis, and wound healing. Polymers (Basel) 2021; 13: 2812.
[20] Zhang M, Wang G, Wang D, Zheng Y, Li Y, Meng W, Zhang X, Du F and Lee S. Ag@MOF-loaded chitosan nanoparticle and polyvinyl alcohol/sodium alginate/chitosan bilayer dressing for wound healing applications. Int J Biol Macromol 2021; 175: 481-494.
[21] Diaz-Gomez L, Gonzalez-Prada I, Millan R, Da Silva-Candal A, Bugallo-Casal A, Campos F, Concheiro A and Alvarez-Lorenzo C. 3D printed carboxymethyl cellulose scaffolds for autologous growth factors delivery in wound healing. Carbohydr Polym 2022; 278: 118924.
[22] Ebrahim N, Dessouky AA, Mostafa O, Hassouna A, Yousef MM, Seleem Y, El Gebaly EAEAM, Allam MM, Farid AS, Saffaf BA, Sabry D, Nawar A, Shoulah AA, Khalil AH, Abdalla SF, El-Sherbiny M, Elsherbiny NM and Salim RF. Adipose mesenchymal stem cells combined with platelet-rich plasma accelerate diabetic wound healing by modulating the notch pathway. Stem Cell Res Ther 2021; 12: 392.
[23] Zheng Z, Li M, Shi P, Gao Y, Ma J, Li Y, Huang L, Yang Z and Yang L. Polydopamine-modified collagen sponge scaffold as a novel dermal regeneration template with sustained release of platelet-rich plasma to accelerate skin repair: a one-step strategy. Bioact Mater 2021; 6: 2613-2628.
[24] Wei S, Xu P, Yao Z, Cui X, Lei X, Li L, Dong Y, Zhu W, Guo R and Cheng B. A composite hydrogel with co-delivery of antimicrobial peptides and platelet-rich plasma to enhance healing of infected wounds in diabetes. Acta Biomater 2021; 124: 205-218.
[25] Qian Z, Wang H, Bai Y, Wang Y, Tao L, Wei Y, Fan Y, Guo X and Liu H. Improving chronic diabetic wound healing through an injectable and self-healing hydrogel with platelet-rich plasma release. ACS Appl Mater Interfaces 2020; 12: 55659-55674.
[26] Cecerska-Heryć E, Goszka M, Serwin N, Roszak M, Grygorcewicz B, Heryć R and Dołęgowska B. Applications of the regenerative capacity of platelets in modern medicine. Cytokine Growth Factor Rev 2022; 64: 84-94.
[27] Kardos D, Simon M, Vácz G, Hinsenkamp A, Holczer T, Cseh D, Sárközi A, Szenthe K, Bánáti F, Szathmary S, Nehrer S, Kuten O, Masteling M, Lacza Z and Hornyák I. The composition of hyperacute serum and platelet-rich plasma is markedly different despite the similar production method. Int J Mol Sci 2019; 20: 721.
[28] Samberg M, Stone R 2nd, Natesan S, Kowalczewski A, Becerra S, Wrice N, Cap A and Christy R. Platelet rich plasma hydrogels promote in vitro and in vivo angiogenic potential of adipose-derived stem cells. Acta Biomater 2019; 87: 76-87.
[29] Xu N, Wang L, Guan J, Tang C, He N, Zhang W and Fu S. Wound healing effects of a curcuma zedoaria polysaccharide with platelet-rich plasma exosomes assembled on chitosan/silk hydrogel sponge in a diabetic rat model. Int J Mol Sci 2018; 117: 102-107.

[30] He X, Liu X, Yang J, Du H, Chai N, Sha Z, Geng M, Zhou X and He C. Tannic acid-reinforced methacrylated chitosan/methacrylated silk fibroin hydrogels with multifunctionality for accelerating wound healing. Carbohydr Polym 2020; 247: 116689.
[31] Ma W, Zhang X, Liu Y, Fan L, Gan J, Liu W, Zhao Y and Sun L. Polydopamine decorated microneedles with Fe-MSC-derived nanovesicles encapsulation for wound healing. Adv Sci (Weinh) 2022; 9: e2103317.
[32] Wang L, Sun L, Bian F, Wang Y and Zhao Y. Self-bonded hydrogel inverse opal particles as sprayed flexible patch for wound healing. ACS Nano 2022; 16: 2640-2650.
[33] Shen J, Chen A, Cai Z, Chen Z, Cao R, Liu Z, Li Y and Hao J. Exhausted local lactate accumulation via injectable nanozyme-functionalized hydrogel microsphere for inflammation relief and tissue regeneration. Bioact Mater 2021; 12: 153-168.
[34] Peng M, Kaczmarek A and Van Hecke K. Ratiometric thermometers based on rhodamine B and fluorescein dye-incorporated (Nano) cyclodextrin metal-organic frameworks. ACS Appl Mater Interfaces 2022; 14: 14367-14379.
[35] Phan-Quang GC, Yang N, Lee HK, Sim HYF, Koh CSL, Kao YC, Wong ZC, Tan EKM, Miao YE, Fan W, Liu T, Phang IY and Ling XY. Tracking airborne molecules from Afar: three-dimensional metal-organic framework-surface-enhanced raman scattering platform for stand-off and real-time atmospheric monitoring. ACS Nano 2019; 13: 12090-12099.
[36] Lu K, Li K, Zhang M, Fang Z, Wu P, Feng L, Deng K, Yu C, Deng Y, Xiao Y, Zhu P and Guo R. Adipose-derived stem cells (ADSCs) and platelet-rich plasma (PRP) loaded gelatin/silk fibroin hydrogels for improving healing in a murine pressure ulcer model. Chem Eng J 2021; 424: 130429.
[37] Bacakova M, Pajorova J, Broz A, Hadraba D, Lopot F, Zavadakova A, Vistejnova L, Beno M, Kostic I, Jencova V and Bacakova L. A two-layer skin construct consisting of a collagen hydrogel reinforced by a fibrin-coated polylactide nanofibrous membrane. Int J Nanomedicine 2019; 14: 5033-5050.
[38] Xie Y, Liao X, Zhang J, Yang F and Fan Z. Novel chitosan hydrogels reinforced by silver nanoparticles with ultrahigh mechanical and high antibacterial properties for accelerating wound healing. Int J Biol Macromol 2018; 119: 402-412.
[39] Xue J, Wang X, Wang E, Li T, Chang J and Wu C. Bioinspired multifunctional biomaterials with hierarchical microstructure for wound dressing. Acta Biomater 2019; 100: 270-279.
[40] Salleh KM, Zakaria S, Sajab MS, Gan S and Kaco H. Superabsorbent hydrogel from oil palm empty fruit bunch cellulose and sodium carboxymethylcellulose. Int J Biol Macromol 2019; 131: 50-59.
[41] Pungrasmi W, Intarasoontron J, Jongvivatsakul P and Likitlersuang S. Evaluation of microencapsulation techniques for MICP bacterial spores applied in self-healing concrete. Sci Rep 2019; 9: 12484.
[42] Asadpour S, Kargozar S, Moradi L, Ai A, Nosrati H and Ai J. Natural biomacromolecule based composite scaffolds from silk fibroin, gelatin and chitosan toward tissue engineering applications. Int J Biol Macromol 2020; 154: 1285-1294.
[43] Brun P, Zamuner A, Battocchio C, Cassari L, Todesco M, Graziani V, Iucci G, Marsotto M, Tortora L, Secchi V and Dettin M. Bio-functionalized chitosan for bone tissue engineering. Int J Mol Sci 2021; 22: 5916.
[44] Hashem HR. Regenerative and antioxidant properties of autologous platelet-rich plasma can reserve the aging process of the cornea in the rat model. Oxid Med Cell Longev 2020; 2020: 4127959.
[45] Wang D, Chen H, Lei L, Chen J, Gao J, Liu J, Li Q, Xie Y, Hu Y and Ni Y. Biofabricated macrophage and fibroblast membranes synergistically promote skin wound healing. Bioeng Transl Med 2022; 7: e10344.
[46] Liu W, Xu B, Xue W, Yang B, Fan Y, Chen B, Xiao Z, Xue X, Sun Z, Shu M, Zhang Q, Shi Y, Zhao Y and Dai J. A functional scaffold to promote the migration and neuronal differentiation of neural stem/progenitor cells for spinal cord injury repair. Biomaterials 2020; 243: 119941.
[47] Zhu Z, Liu Y, Chen J, He Z, Tan P, He Y, Pei X, Wang J, Tan L and Wan Q. Structural-functional pluralistic modification of silk fibroin via MOF bridging for advanced wound care. Adv Sci (Weinh) 2022; 9: e2204553.
[48] Ma R, Wu P, Shi Q, Song D and Fang H. Telocytes promote VEGF expression and alleviate ventilator-induced lung injury in mice. Acta Biochim Biophys Sin (Shanghai) 2018; 50: 817-825.
[49] Xiong Y, Xu Y, Zhou F, Hu Y, Zhao J, Liu Z, Zhai Q, Qi S, Zhang Z and Chen L. Bio-functional hydrogel with antibacterial and anti-inflammatory dual properties to combat with burn wound infection. Bioeng Transl Med 2022; 8: e10373.
[50] Veith AP, Henderson K, Spencer A, Sligar AD and Baker AB. Therapeutic strategies for enhancing angiogenesis in wound healing. Adv Drug Deliv Rev 2019; 146: 97-125.
[51] Piperigkou Z, Götte M, Theocharis AD and Karamanos NK. Insights into the key roles of epigenetics in matrix macromolecules-associ-

ated wound healing. Adv Drug Deliv Rev 2018; 129: 16-36.
[52] Blume PA, Walters J, Payne W, Ayala J and Lantis J. Comparison of negative pressure wound therapy using vacuum-assisted closure with advanced moist wound therapy in the treatment of diabetic foot ulcers: a multicenter randomized controlled trial. Diabetes Care 2008; 31: 631-636.
[53] Henriques-Antunes H, Cardoso RMS, Zonari A, Correia J, Leal EC, Jiménez-Balsa A, Lino MM, Barradas A, Kostic I, Gomes C, Karp JM, Carvalho E and Ferreira L. The kinetics of small extracellular vesicle delivery impacts skin tissue regeneration. ACS Nano 2019; 13: 8694-8707.
[54] Becker RC, Sexton T and Smyth SS. Translational implications of platelets as vascular first responders. Circ Res 2018; 122: 506-522.
[55] Ziaei M, Greene C and Green CR. Wound healing in the eye: therapeutic prospects. Adv Drug Deliv Rev 2018; 126: 162-176.
[56] Chen S, Li R, Li X and Xie J. Electrospinning: an enabling nanotechnology platform for drug delivery and regenerative medicine. Adv Drug Deliv Rev 2018; 132: 188-213.
[57] Yamamoto M, Sato T, Beren J, Verthelyi D and Klinman DM. The acceleration of wound healing in primates by the local administration of immunostimulatory CpG oligonucleotides. Biomaterials 2011; 32: 4238-4242.